Dynamics of Strong-Field Double Ionization in Two-Color Counterrotating Fields

Jan L. Chaloupka[1] and Daniel D. Hickstein[2]

[1]*Department of Physics and Astronomy, University of Northern Colorado, Greeley, Colorado 80639, USA*
[2]*JILA–Department of Physics, University of Colorado and NIST, Boulder, Colorado 80309, USA*

The double ionization of helium in bichromatic, circularly polarized intense laser fields is analyzed with a classical ensemble approach. It is found that counterrotating fields produce significant nonsequential double-ion yield and drive novel ionization dynamics. It is shown that distinct pathways to ionization can be modified by altering the relative intensities of the two colors, allowing for unique control of strong-field processes. Electrons are observed to return to the ion at different angles from the angle of ionization, opening new possibilities for probing electronic and molecular structure on the ultrafast time scale.

In the years following the initial observation of strong-field ionization [1,2], a simple and powerful interpretation known as rescattering was developed that has helped guide researchers for decades [3–6]. In this three-step (or simple-man's) model, the intense laser field sufficiently distorts the atomic Coulomb potential, allowing a single electron to be liberated by tunnel ionization. The electron gains energy from the oscillating laser field and can be driven back to the ion, leading to release of the second electron. This process results in nonsequential double ionization (NSDI) [7–9] and is most effective with linear polarization, where the electron trajectories return strongly to the parent ion, and is significantly suppressed with circular polarization [8,10].

In this Letter, we present an analysis of NSDI in two-color, circularly polarized, counterrotating fields. These fields [11–13] have been successfully used to drive high-harmonic generation (HHG) [14–16], allowing for the direct generation of circularly polarized soft x-ray pulses, and spurring interest in the ultrafast electron dynamics in such fields. In this investigation, we employ the ensemble approach utilizing a classical model atom, as pioneered by Eberly and Haan [17–20]. Not only does this theoretical technique provide excellent qualitative agreement with experimentally observed features, it also gives clear and intuitive insight to the underlying processes and helps to guide future experiments, and the use of large ensembles of randomized model atoms mimics some quantum effects, such as wave-packet spreading. We present, for the first time, an analysis of the ion yield curves, the electron energy and momentum distributions, and electron timing information from NSDI with two-color circular fields. We uncover a unique diversity in the pathways leading to rescattering, including electron dynamics that are not possible with linear polarization, and we show how these mechanisms vary with the relative intensity of the two colors. Importantly, we find that it is possible to drive electrons in complex trajectories and return them to the ion at impact angles very different from the angle of release, thereby

opening new possibilities for photoelectron [21,22] and high-harmonic [23,24] spectroscopies, where the returning electron can be used to probe the atomic or molecular structure of the parent ion.

The results presented here were generated using a three-dimensional numerical simulation of a realistic laser pulse interacting with a classical model helium atom. The laser pulse is focused to a beam waist of 10 μm with the model atom placed at the center of the focus, and has a Gaussian pulse width of 10 fs with zero carrier-envelope phase. The full three dimensions of the electric and magnetic fields are included up to first order [25]. The model atom softening parameters and the method of randomization for each computational run are described in detail elsewhere [19,26]. In general, we employ the so-called Rochester potential, where the Coulomb potential is modified with softening terms to avoid autoionization while maintaining proper field-ionization behavior, and the initial electron positions and momenta are randomized while ensuring the correct helium bound state energy. For a given intensity and field structure, ensembles of 10^5 or 10^6 randomized model atoms are used. Also, throughout this Letter, the peak electric field amplitude is held fixed for a given set of simulations, as field amplitude is the relevant parameter for determining the ionization probability. This scaling choice allows for the direct comparison between linearly polarized and two-color circularly polarized results. However, since it is common practice to use an intensity (rather than an amplitude) scale, we report our results in terms of the intensity of linearly polarized light corresponding to that same peak field amplitude.

In Fig. 1, the single- and double-ionization ion yield curves are shown for a variety of conditions. Using either single-color linear polarization or two-color counterrotating circular polarization, an NSDI "knee" region of enhanced double-ion yield is universally observed. As a result of scaling according to field amplitude, all of the single ion yield curves (He^{1+}) are nearly identical, allowing
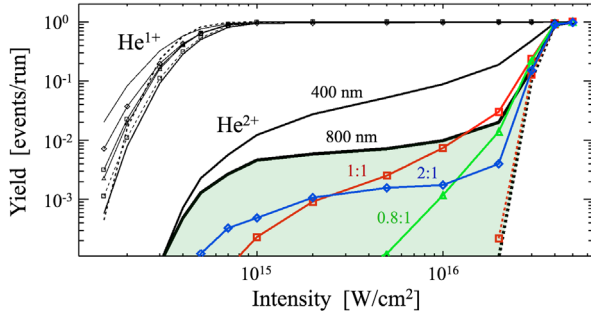
FIG. 1.   Ion yield curves show NSDI enhancement for single-color linear polarization (800 nm, thick solid line; 400 nm, thin solid line) and two-color counterrotating cases (solid lines with symbols), but not for circular polarization or corotating cases (dashed lines). The shape of the double-ion yield curve varies considerably with the 400∶800 nm amplitude ratios—0.8 (green triangles), 1.0 (red squares), and 2.0 (blue diamonds). The region of 800 nm NSDI enhancement is shaded. Each data point represents 10^5 simulations runs.
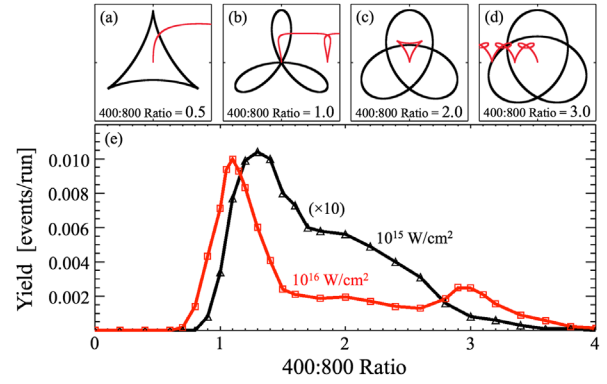

FIG. 2.   (a)–(d) Electric field amplitudes (black lines, arbitrary units) driving electron trajectories (red lines, arbitrary units) for a range of 400∶800 amplitude ratios. In this simple model, which assumes ionization at the peak of the field and ignores the Coulomb potential, perfect returning paths are seen only for a ratio of 2.0. (e) Double ion production from the full simulation versus 400∶800 amplitude ratio for 10^{15} and 10^{16} W/cm². Each data point represents 10^5 simulations runs.

for a direct comparison of the double ionization (He^{2+}) behavior. The presence of NSDI is observed in our simulations for a broad range of 400∶800 nm field ratios, as well as for other wavelengths of counterrotating light (not presented here), but suppressed in corotating cases. By changing the 400∶800 field ratio, the NSDI knee shape is altered, but the existence of NSDI persists. While the change in shape of the knee is not, on its own, enough to determine the underlying double ionization dynamics, it is an indication that more than a single NSDI mechanism may be at work, just as the original observation of the NSDI knee indicated two distinct rates, corresponding to the sequential and direct processes.

As shown in Fig. 2(e), a broad range of enhanced NSDI yield is observed from our full simulations for ratios between 0.7∶1 and 4∶1. This is somewhat surprising, considering the simple trajectories [red lines in Figs. 2(a)–(d)] of an electron released at rest at the peak of the electric field (black lines), with no effect from the Coulomb potential included. For low ratio values [Fig. 2(a)], the behavior is similar to that of ordinary circular polarization, where the electron is driven far from its original location. Not surprisingly, there is no double ionization signal. As the ratio is increased [Fig. 2(b)], the electron is still driven away from the origin, but now short, looping paths appear in the electron trajectory. At a ratio of 2.0 [Fig. 2(c)] the electron returns repeatedly in a perfect triangular trajectory. Finally, for higher ratio values [Fig. 2(d)], elaborate looping trajectories are observed, but electrons are not driven back to the ion. Considering only this simplified approach, one might expect that NSDI should only be observed for ratio values of about 2, since this is where closed-loop, returning trajectories are observed. However, the full simulations reveal that NSDI is highest at a ratio of ~1, indicating that more complex

factors (e.g., phase of release, initial electron momentum, and effect of the Coulomb potential) play an important role in determining the double-ionization dynamics. All of these factors are inherently a part of the full simulation results presented throughout this Letter, as the classical model atoms are under the sole influence of the evolving laser pulse without any artificial choice of release phase, momentum, or other parameters. The randomization of both of the electrons' positions and momenta occurs at the very beginning of the simulation, where the electrons are still bound and the laser pulse is off, and all subsequent behavior, including ionization and rescattering, is due only to the electron-ion, electron-electron, and electron-laser interaction.

To better understand the underlying NSDI behavior, we present He^{1+} and He^{2+} electron energies, momentum distributions, and timing information for four cases (Fig. 3, all at 10^{16} W/cm²) with ensembles of 10^6 simulation runs. The electron energy distribution from linearly polarized light [Fig. 3(a)] shows the familiar cutoff at $2U_p$ for He^{1+} electrons and a significant extension to higher energies for He^{2+} electrons, as expected [27]. The electron momentum distributions in the transverse plane are plotted for He^{1+} [Fig. 3(b)] and He^{2+} [Fig. 3(c)] electrons, and demonstrate that rescattering leads to higher momenta for electrons correlated to He^{2+}. In Fig. 3(d), the "recollision timing" information is shown, where the double-ionization yield is plotted versus the time difference between single ionization (the time when the total energy of the first electron is greater than zero) and impact (the time of closest return). The first, largest peak corresponds to electrons returning at roughly one-half of an optical cycle, and represents the standard mechanism of rescattering, and the peaks at longer times correspond to multiple
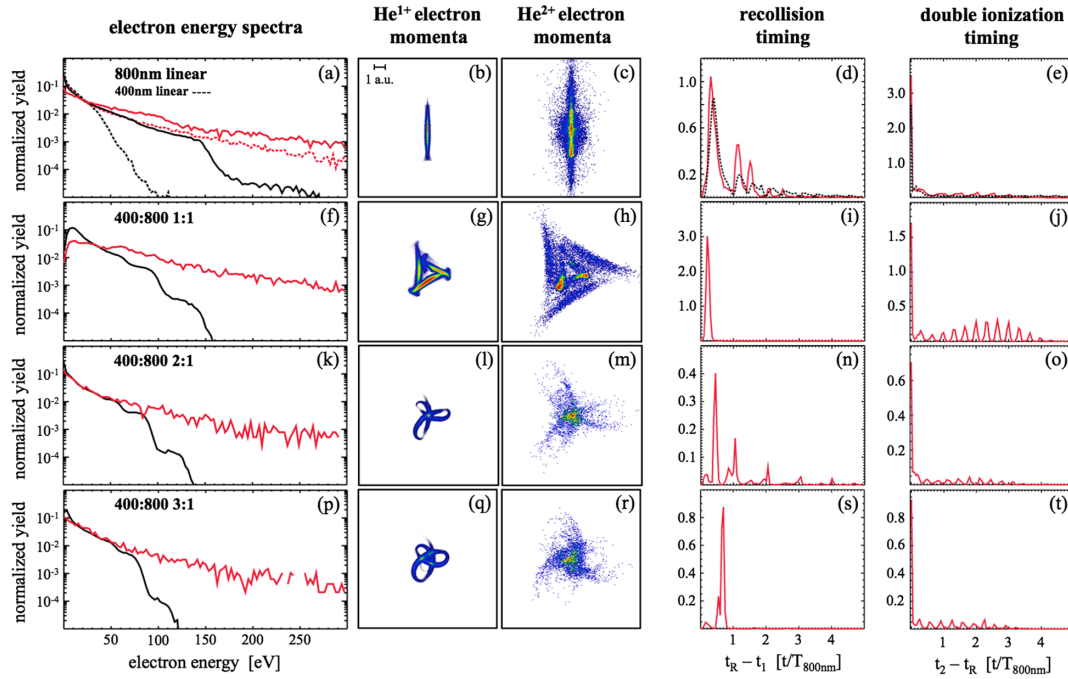
FIG. 3.   Electron energy and momentum distributions and ionization timing are shown for four cases: 800 nm linear polarization (first row, with 400 nm linear results shown as dashed lines), 1:1 ratio of 400:800 nm counterrotating light (second row), 2:1 mix (third row), 3:1 mix (fourth row); corotating fields result in minimal double ionization events. The columns show electron energy distributions (where the total yield is normalized to one for each curve), transverse electron momentum distributions corresponding to He^{1+} and He^{2+} ion production, and recollision and double ionization timing (double-ion yield is displayed in arbitrary units, but the scale is the same for all plots, and time is displayed in terms of 800 nm optical cycles). The 400 nm linear polarization timing results are scaled (in time and yield) for comparison to the 800 nm curves. For each row, 10^6 simulation runs were used.

returns. In Fig. 3(e), the "double ionization timing" is shown, where the double-ion yield is plotted versus the time difference between impact of the first electron and the subsequent release of the second electron. The sharp peak at zero corresponds to an immediate release (impact ionization), while the structure at longer times corresponds to a delayed release (impact excitation followed by field ionization).

In the second row, results for a 1:1 mix of 400:800 light show pronounced differences compared to the linearly polarized case. In Fig. 3(f), the He^{1+} electron energies show more complex structure due to the bichromatic driving field, while the He^{2+} electrons exhibit the high-energy distribution indicative of rescattering. Both curves show a reduction in low-energy electrons, which is caused by the quasielliptical lobes in the E field imparting extra drift momentum to the electrons. Since the timing of the electron release affects not only the magnitude of the electron's momentum, but also the direction (similar to elliptical polarization [28]), a complex pattern is formed in the He^{1+} [Fig. 3(g)] and He^{2+} [Fig. 3(h)] electron momentum distributions. The impact timing shown in Fig. 3(i) has only one peak at roughly 0.2 optical cycles. This shows that rescattering can occur on a very short time scale (even shorter than with linear polarization), and need not be due to the full-cycle structure of the field. This also

indicates why two-color, counterrotating fields in general will generate NSDI for a broad range of conditions, as rescattering can occur due to the dynamics of the subcycle nature of the field and does not necessarily rely on the presence of perfect, full-cycle returning trajectories. As shown in Fig. 3(j), an increase in excitation followed by field ionization is observed. This implies that the momentum of the returning electrons is often not sufficient for direct impact ionization, leaving more instances of excited atoms available for eventual field ionization.

In the case of a 2:1 400:800 ratio (Fig. 3, third row), the He^{2+} electron distributions extend to high energies [Fig. 3(k)], but now a low-energy peak in both the He^{1+} and He^{2+} distributions is present, since electrons released at the peak of the field can return with zero energy one cycle later [the triangle-shaped trajectory in Fig. 2(c)]. Accordingly, the He^{1+} [Fig. 3(l)] and He^{2+} [Fig. 3(m)] momentum distributions exhibit a low momentum peak surrounded by more complex structure. In Fig. 3(n), the rescattering timing is significantly more complex, with peaks corresponding to a range of return times due to subcycle, single-cycle, and multicycle trajectories. Also, immediate double ionization following rescattering is very common [Fig. 3(o)], indicating that electrons are returning to the ion with sufficient momentum to effectively drive impact ionization. Finally, the fourth row of Fig. 3 shows results
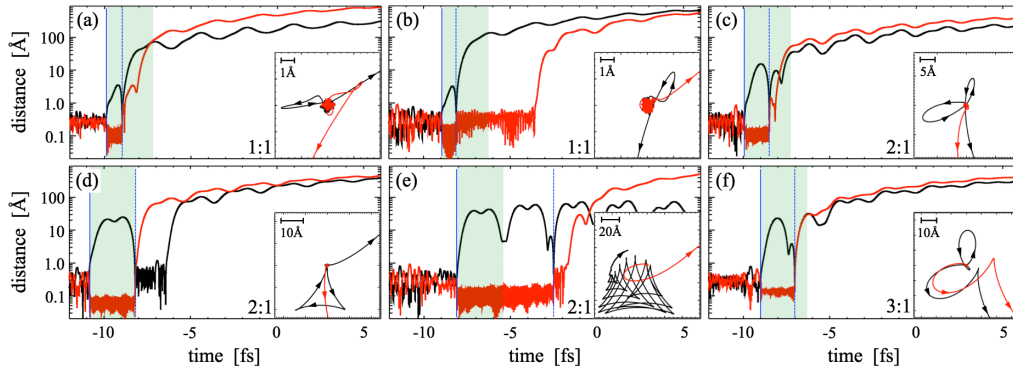
FIG. 4.   Sample electron trajectories for six cases show electron distance from the ion versus time, as well as a transverse view of the electrons' path (inset): (a),(b) Short excursions from a 1:1 mix of 400:800 light, (c) subcycle path from a 2:1 mix, (d) full-cycle path from a 2:1 mix, (e) two-cycle path from a 2:1 mix, and (f) subcycle path from a 3:1 mix. The first electron's release time (solid blue line) and impact time (dashed blue line) is shown in each panel, along with the timing of a single optical cycle (shaded).

for a 3:1 400:800 ratio. The electron energy distributions [Fig. 3(p)] and He^{1+} [Fig. 3(q)] and He^{2+} [Fig. 3(r)] momentum distributions are similar to the 2:1 mix, but the rescattering timing information [Fig. 3(s)] shows only one major peak. Since this occurs at less than one optical cycle, it indicates that a subcycle portion of the trajectory shown in [Fig. 2(d)] is contributing to this process. As is readily apparent from these four examples, a significant shift in ionization dynamics can be induced by simply altering the amplitude ratio of the two counterrotating fields.

In order to provide additional, intuitive insights into the dynamics of NSDI in counterrotating fields, we present several representative electron trajectories from our simulations. In Fig. 4, the electron-ion distance is shown for each electron as a function of time, and a transverse view of the trajectories is shown in the inset panel. An impact ionization event [Fig. 4(a)] and an excitation-and-field-ionization event [Fig. 4(b)] are shown for a 1:1 mix of 400:800 light. In both cases, the first electron makes a very short looping excursion in the field before impacting at a different angle than its angle of release. Next, sample events from the 2:1 mix help to demonstrate the diversity of rescattering processes possible, as indicated by the timing information shown in Fig. 3(n). An example of a short, subcycle trajectory [Fig. 4(c)] corresponds to the tall peak at roughly 0.5 cycles in Fig. 3(n), while a one-cycle return [Fig. 4(d)] and a two-cycle return [Fig. 4(e)] correspond to the peaks at approximately one and two optical cycles. The latter trajectory exhibits several subsequent returns, ending in a near-zero final energy for that electron. Finally, a trajectory for a 3:1 mix is shown in Fig. 4(f). Even though the 3:1 combination of fields does not produce a full-cycle closed-loop path in the simplest model [Fig. 3(d)], in the full simulation it clearly does generate an efficient looping trajectory with subcycle timing, resulting in the bump in double-ion yield in Fig. 2(e).

These specific examples of NSDI events allow us to visualize the subcycle, single-cycle, and multicycle

dynamics that are possible with bichromatic, counterrotating fields. We also demonstrate that the relative importance of each type of path can be adjusted via the amplitude ratio of the 400 and 800 nm fields. At low ratio values, none of these are possible. At around a 1:1 ratio, subcycle returns are observed. With higher ratio values, longer paths begin to play a role, with a peak in full-cycle and multicycle trajectories at a 2:1 ratio, and a favorable subcycle path occurring at a 3:1 ratio. Finally, for ratios larger than 4:1, all NSDI processes shut down. Evidence for these processes can be readily verified in the lab. In fact, enhanced double-ion yield for counterrotating fields has been recently recorded [29], and the existence of closed-loop trajectories can be determined by simply looking for a peak in the production of low-energy photoelectrons. Of course, advanced techniques such as COLTRIMS can be used to record complete He^{1+} and He^{2+} photoelectron momenta [30], allowing for sophisticated and direct comparison to our results. Also, since the presence of these complex trajectories relies on the driving field configuration and not the atomic species, similar behavior should be observed for high-Z atoms and molecules.

The work presented here represents an important departure from typical strong-field double-ionization phenomena. The electron trajectories driven by two-color counterrotating fields are complex and their shape varies significantly depending on the makeup of the driving field. The resulting electron momenta are spread throughout the transverse plane, enabling sophisticated analysis of both the tunnel ionization and rescattering processes. The angle of electron impact is shown to be very different from the angle of release, and the excursion time exhibits a remarkable diversity, from subcycle to single-cycle to multicycle time scales. Understanding the details of this behavior represents a significant opportunity for future theoretical and experimental study, and provides a promising avenue for the tunable control of strong-field processes. We are grateful

———————

[1] G. S. Voronov and N. B. Delone, Many-photon ionization of the xenon atom by ruby laser radiation, Sov. Phys. JETP **23**, 54 (1966).

[2] P. Agostini, F. Fabre, G. Mainfray, G. Petite, and N. K. Rahman, Free-free transitions following six-photon ionization of xenon atoms, Phys. Rev. Lett. **42**, 1127 (1979).

[3] M. Yu Kuchiev, Atomic antenna, JETP Lett. **45**, 404 (1987).

[4] P. B. Corkum, Plasma perspective on strong field multiphoton ionization, Phys. Rev. Lett. **71**, 1994 (1993).

[5] K. J. Schafer, B. Yang, L. F. DiMauro, and K. C. Kulander, Above threshold ionization beyond the high harmonic cutoff, Phys. Rev. Lett. **70**, 1599 (1993).

[6] W. Becker, X. Liu, P. J. Ho, and J. H. Eberly, Theories of photoelectron correlation in laser-driven multiple atomic ionization, Rev. Mod. Phys. **84**, 1011 (2012).

[7] A. l'Huillier, L. A. Lompre, G. Mainfray, and C. Manus, Multiply charged ions induced by multiphoton absorption in rare gases at 0.53 μm, Phys. Rev. A **27**, 2503 (1983).

[8] D. N. Fittinghoff, P. R. Bolton, B. Chang, and K. C. Kulander, Observation of nonsequential double ionization of helium with optical tunneling, Phys. Rev. Lett. **69**, 2642 (1992).

[9] B. Walker, B. Sheehy, L. F. DiMauro, P. Agostini, K. J. Schafer, and K. C. Kulander, Precision measurement of strong field double ionization of helium, Phys. Rev. Lett. **73**, 1227 (1994).

[10] P. Dietrich, N. H. Burnett, M. Ivanov, and P. B. Corkum, High-harmonic generation and correlated two-electron multiphoton ionization with elliptically polarized light, Phys. Rev. A **50**, R3585 (1994).

[11] D. B. Milošević, W. Becker, and R. Kopold, Generation of circularly polarized high-order harmonics by two-color coplanar field mixing, Phys. Rev. A **61**, 063403 (2000).

[12] A. Kramo, E. Hasović, D. B. Milošević, and W. Becker, Above-threshold detachment by a two-color bicircular laser field, Laser Phys. Lett. **4**, 279 (2007).

[13] S. Odžak and D. B. Milošević, Bicircular-laser-field-assisted electron-ion radiative recombination, Phys. Rev. A **92**, 053416 (2015).

[14] H. Eichmann, A. Egbert, S. Nolte, C. Momma, B. Wellegehausen, W. Becker, S. Long, and J. K. McIver, Polarization-dependent high-order two-color mixing, Phys. Rev. A **51**, R3414 (1995).

[15] A. Fleischer, O. Kfir, T. Diskin, P. Sidorenko, and O. Cohen, Spin angular momentum and tunable polarization in high-harmonic generation, Nat. Photonics **8**, 543 (2014).

[16] O. Kfir, P. Grychtol, E. Turgut, R. Knut, D. Zusin, D. Popmintchev, T. Popmintchev, H. Nembach, J. M. Shaw, A. Fleischer, H. Kapteyn, M. Murnane, and O. Cohen, Generation of bright phase-matched circularly-polarized extreme ultraviolet high harmonics, Nat. Photonics **9**, 99 (2015).

[17] R. Panfili, S. L. Haan, and J. H. Eberly, Slow-down collisions and nonsequential double ionization in classical simulations, Phys. Rev. Lett. **89**, 113001 (2002).

[18] P. J. Ho, R. Panfili, S. L. Haan, and J. H. Eberly, Nonsequential double ionization as a completely classical photoelectric effect, Phys. Rev. Lett. **94**, 093002 (2005).

[19] S. L. Haan, L. Breen, A. Karim, and J. H. Eberly, Variable time lag and backward ejection in full-dimensional analysis of strong-field double ionization, Phys. Rev. Lett. **97**, 103008 (2006).

[20] S. L. Haan, J. S. Van Dyke, and Z. S. Smith, Recollision excitation, electron correlation, and the production of high-momentum electrons in double ionization, Phys. Rev. Lett. **101**, 113001 (2008).

[21] C. I. Blaga, J. Xu, A. D. DiChiara, E. Sistrunk, K. Zhang, P. Agostini, T. A. Miller, L. F. DiMauro, and C. D. Lin, Imaging ultrafast molecular dynamics with laser-induced electron diffraction, Nature (London) **483**, 194 (2012).

[22] J. Xu, C. I. Blaga, K. Zhang, Y. H. Lai, C. D. Lin, T. A. Miller, P. Agostini, and L. F. DiMauro, Diffraction using laser-driven broadband electron wave packets, Nat. Commun. **5**, 4635 (2014).

[23] W. Li, X. Zhou, R. Lock, S. Patchkovskii, A. Stolow, H. C. Kapteyn, and M. M. Murnane, Time-resolved dynamics in N_2O_4 probed using high harmonic generation, Science **322**, 1207 (2008).

[24] C. Jin, J. B. Bertrand, R. R. Lucchese, H. J. Wörner, P. B. Corkum, D. M. Villeneuve, A.-T. Le, and C. D. Lin, Intensity dependence of multiple orbital contributions and shape resonance in high-order harmonic generation of aligned N_2 molecules, Phys. Rev. A **85**, 013405 (2012).

[25] L. W. Davis, Theory of electromagnetic beams, Phys. Rev. A **19**, 1177 (1979).

[26] J. P. Paquette and J. L. Chaloupka, Effect of realistic focal conditions on the strong-field ionization of helium, Phys. Rev. A **79**, 043410 (2009).

[27] R. Lafon, J. L. Chaloupka, B. Sheehy, P. M. Paul, P. Agostini, K. C. Kulander, and L. F. DiMauro, Electron energy spectra from intense laser double ionization of helium, Phys. Rev. Lett. **86**, 2762 (2001).

[28] X. Wang and J. H. Eberly, Classical theory of high-field atomic ionization using elliptical polarization, Phys. Rev. A **86**, 013421 (2012).

[29] C. A. Mancuso, K. M. Dorney, J. L. Chaloupka, J. L. Ellis, F. J. Dollar, R. Knut, P. Grychtol, D. Zusin, C. Gentry, H. C. Kapteyn, M. M. Murnane, and D. D. Hickstein, Nonsequential double ionization in two-color circularly polarized femtosecond laser fields (to be published).

[30] A. Rudenko, V. L. B. de Jesus, Th. Ergler, K. Zrost, B. Feuerstein, C. D. Schröter, R. Moshammer, and J. Ullrich, Correlated two-electron momentum spectra for strong-field nonsequential double ionization of He at 800 nm, Phys. Rev. Lett. **99**, 263003 (2007).